Title: Response of intestinal HT-29 cells to the trichothecene mycotoxin deoxynivalenol and its sulfated conjugates

Authors: Giorgia Del Favero, Lydia Woelflingseder, Dominik Braun, Hannes Puntscher, Mary-Liis Kütt, Luca Dellafiora, Benedikt Warth, Gudrun Pahlke, Chiara Dall'Asta, Gerhard Adam, Doris Marko

PII: S0378-4274(18)31491-7
DOI: https://doi.org/10.1016/j.toxlet.2018.07.007
Reference: TOXLET 10265

To appear in: *Toxicology Letters*

Received date: 17-4-2018
Revised date: 3-7-2018
Accepted date: 5-7-2018

Please cite this article as: Favero GD, Woelflingseder L, Braun D, Puntscher H, Kütt M-Liis, Dellafiora L, Warth B, Pahlke G, Dall'Asta C, Adam G, Marko D, Response of intestinal HT-29 cells to the trichothecene mycotoxin deoxynivalenol and its sulfated conjugates, *Toxicology Letters* (2018), https://doi.org/10.1016/j.toxlet.2018.07.007

Response of intestinal HT-29 cells to the trichothecene mycotoxin deoxynivalenol and its sulfated conjugates

Giorgia Del Favero[1], Lydia Woelflingseder[1], Dominik Braun[1], Hannes Puntscher[1], Mary-Liis Kütt[1], Luca Dellafiora[2], Benedikt Warth[1], Gudrun Pahlke[1], Chiara Dall'Asta[2], Gerhard Adam[3], Doris Marko[1*]

[1]University of Vienna, Department of Food Chemistry and Toxicology, Währingerstr. 38, 1090 Vienna, Austria

[2]Department of Food and Drug, University of Parma, Via G.P. Usberti 27/A, 43124 Parma, Italy

[3]University of Natural Resources and Life Sciences, Vienna (BOKU), Department of Applied Genetics and Cell Biology-, Konrad-Lorenz-Str. 24, 3430 Tulln, Austria

* Corresponding author: Prof. Dr. Doris Marko (doris.marko@univie.ac.at)

Department of Food Chemistry and Toxicology, Faculty of Chemistry, University of Vienna. Währingerstr. 38-40, 1090 Vienna, Austria.

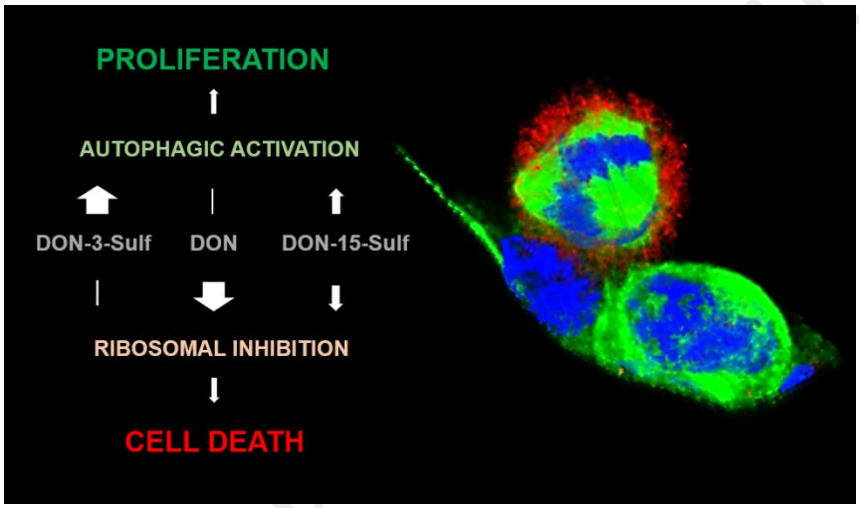

Toxicity of trichothecene mycotoxin deoxynivalenol (DON) and its sulfated metabolites differ in HT-29 cells. Combined *in vitro*/*in silico* approach was used to explore the differential pathways activated by DON-3-sulfate and DON-15-sulfate in comparison to the parent compound in intestinal cells.

Highlights

- DON-3- Sulf and DON-15-Sulf are taken up by HT-29 cells, but less compared to DON
- *In silico* modelling show lacking fit of DON-sulfates to the ribosomal pocket
- DON-3- Sulf and DON-15-Sulf mediate a proliferative stimulus and activate autophagy

Deoxynivalenol (DON); Deoxynivalenol-3-sulfate (DON-3-Sulf); Deoxynivalenol-15-sulfate (DON-15-Sulf); Glyceraldehyde 3-phosphate dehydrogenase (GAPDH), Kelch-like ECH-associated protein 1 (Keap-1), Nuclear factor (erythroid-derived 2)-like 2 (Nrf-2) Gamma-glutamate-cysteine ligase (γ-GCL), NAD(P)H dehydrogenase quinine 1 (NQO-1) and interleukin 8 (IL-8), Cyclooxygenase 2 (Cox-2).

Abstract

The sulfated forms of the *Fusarium* toxin deoxynivalenol (DON), deoxynivalenol-3-sulfate (DON-3-Sulf) and deoxynivalenol-15-sulfate (DON-15-Sulf) were recently described, however little is known about their mechanism of action in mammalian cells. DON-3-Sulf and DON-15-Sulf were taken up by HT-29 colon carcinoma cells, although to a lesser extent compared to DON. All three compounds were found to enhance the intracellular ROS level in the dichlorofluorescein assay (≥ 1µM), even though substantial differences were observed in their cytotoxic potential. *In silico* modelling highlighted that DON-sulfates do not share the classical mechanism of action of DON, being unable to fit into the ribosomal pocket and trigger the classical ribotoxic stress response. However, DON-3-Sulf and DON-15-Sulf sustained a distinctive proliferative stimulus in HT-29 and activated autophagy. The mechanisms of action of DON-3-Sulf and DON-15-Sulf suggest a potential interplay between the onset of ribosomal inhibition and autophagy activation as an alternative and/or complementary mode of action for DON and its sulfated analogues.

Abbreviations:

Graphical Abstract

Keywords: Deoxynivalenol-3-sulfate; Deoxynivalenol-15-sulfate; Cell proliferation; Food contaminant mycotoxins; Cytotoxicity

1. Introduction

Over the last decades, food quality and safety have become topics of primary importance. Optimization of agricultural practice, storage conditions and packaging aim to increase the availability and the quality of food items in a globalized world. Despite all efforts, food contamination by mycotoxins still represents a major threat for consumers, and remains a key challenge for food safety (European Food Safety 2013). The trichothecene deoxynivalenol (DON, vomitoxin) is one of the most prevalent mycotoxins, particularly in regions of temperate climate and it is regularly found in cereals worldwide (Li et al. 2016; Liu et al. 2016; Tima et al. 2016; Tralamazza et al. 2016a; Tralamazza et al. 2016b). In fact, together with other trichothecenes, DON is produced by several fungi of the *Fusarium species complex* (van der Lee et al. 2015). At the molecular level, trichothecene mycotoxins are known to block protein synthesis (Cundliffe et al. 1974; Ueno 1977) and, in particular, to bind to the 60S large subunit of the ribosomes inhibiting peptidyl-transferase activity. This event triggers, at cellular level, the so-called "ribotoxic stress response" that ultimately may lead to irreversible cell damage (Pestka 2010b). In mammals, exposure to DON results in a complex pathophysiology, whereby the severity depends on the dose and the duration of the toxic insult. Acute intoxications affect primarily the gastrointestinal tract with symptoms ranging from initial nausea and malaise to more severe manifestations like emesis and diarrhea (Pinton and Oswald 2014), as repeatedly reported also in animals (Danicke and Brezina 2013) and humans (Bhat et al. 1989; Li et al. 1999). Despite the knowledge about DON and analogues, many aspects concerning the toxicity and metabolism of DON remain to be addressed. DON is known to be metabolized in mammalian cells with glucuronidation representing the predominant metabolic pathway (Maul et al. 2012; Sarkanj et al. 2013; Turner et al. 2011; Warth et al. 2012). Beside respective glucuronides, DON has been recently found in human urine also as sulfate conjugate at the C-3 position (DON-3-sulfate) (Warth et al. 2016). Moreover, DON-3-sulfate (DON-3-Sulf) and DON-15-sulfate (DON-15-Sulf) were identified as plant metabolites (Schmeitzl et al. 2015; Warth et al. 2015), suggesting that exposure to these newly identified modified mycotoxins, albeit in a low concentration range, may be relevant to humans. Recent studies

demonstrated that the two sulfated metabolites do not share the high affinity of DON for the ribosome (Warth et al. 2016; Warth et al. 2015) and, accordingly, they lack a direct cytotoxic potential. However, surprisingly, DON-3-Sulf and DON-15-Sulf sustain a distinctive proliferative stimulus in cancer cells (Warth et al. 2016) raising the question on the underlying mechanism of action.

The activity of DON-3-Sulf and DON-15-Sulf was taken as a benchmark for the investigation of the similarities and the differences between the metabolites and the parent toxin DON. Experiments were performed in HT-29 colon cancer cells, which represents a well-established *in vitro* model for intestinal cells, often used as one of the first steps in toxicity studies. The activity of DON-3-Sulf and DON-15-Sulf was described from the uptake at cellular level and up to the molecular mechanism of action. To this aim, classical *in vitro* toxicology was combined with analytical chemistry, molecular biology and *in silico* modelling and the sum of these experiments lead ultimately to propose an alternative mode of action for trichothecene mycotoxins. This pathway acting downstream of direct ribosomal inhibition, at moderately inhibitory concentrations possibly sustains the proliferative effect caused not only by DON-3-Sulf and DON-15-Sulf (Warth et al. 2016), but also by DON, though in a very limited concentration range (Manda et al. 2015; Warth et al. 2016).

2. *Materials and Methods*

2.1. Cell culture conditions

The human colon adenocarcinoma cell line HT-29 (ATCC cat. nr: HTB-38^{TM}) was cultivated in Dulbecco Modified Eagle Medium (DMEM) with 10 % fetal calf serum (FCS) and 1 % penicillin/streptomycin (P/S, 50 U/ml). Cell culture media and supplements were purchased from GIBCO Invitrogen (Karlsruhe, Germany), Lonza Group Ltd (Basel, Switzerland), Sigma-Aldrich Chemie GmbH (Munich, Germany), Sarstedt AG & Co (Nuembrecht, Germany), VWR International GmbH (Vienna, Austria), Fisher Scientific (Austria) GmbH (Vienna, Austria) and Szabo-Scandic Handels GmbH & Co KG (Vienna, Austria). For cell cultivation and incubations humidified incubators at 37 °C and 5 % CO_2 were used and cells were regularly tested for absence of mycoplasm contamination. DON was purchased from Romerlabs (Tulln, Austria); DON-3-Sulf and DON-15-Sulf were synthesized in house as previously described (Fruhmann et al. 2014a). The purity of both DON-sulfates was >95% and determined by NMR. All compounds were dissolved in water.

2.2. Evaluation of cellular uptake

2.2.1 Sample preparation

HT-29 cells were seeded in 6 well-plates (750,000 cells/well), grown for 48 h and incubated for additional 24 h with DON or its modified forms at a concentration of 10 µM or bi-distilled H_2O (negative control). Following incubation, 0.2 mL of the culture medium were transferred into reaction tubes containing 0.8 mL of ice cold extraction solvent (ACN/MeOH; 1:1, v/v). Subsequently, the tubes were incubated at -20˚C for 1 h and centrifuged for 15 min (4˚C) to precipitate proteins. The supernatant was transferred to new reaction tube, evaporated to dryness using a Labconco Centrivap Benchtop Vacuum Concentrator (Labconco, USA). Extracts were reconstituted in 1 mL of dilution solvent (MeOH/water; 1:9, v/v), centrifuged (15 min at 18.400 rcf 4˚C), transferred to an HPLC vial and stored at 4°C until LC-MS/MS analysis. To evaluate intracellular toxin concentrations, cell extracts were prepared. Cells were washed twice with pre-warmed PBS and scraped after adding 1 mL of ice cold

quenching solution (ACN/MeOH/water; 4:4:2, v/v) and transferred into reaction tubes. Subsequently, 2 cycles of thermal lysis were performed as follows: *i)* vortex 30 s *ii*) liquid nitrogen 1 min *iii*) water bath 37 °C 5 min *iiii)* sonication in ice water 10 min. Samples were then incubated for 1 h at -20°C, and centrifuged 15 min at 18.400 rcf (4°C). The resulting supernatant was removed and evaporated to dryness as described above. The dried extracts were reconstituted in MeOH/water (1:9, v/v) and normalized according to the protein concentration determined by the BCA assay. Thereafter, samples were centrifuged for 15 min at 18.400 rcf, 4 °C and the supernatants were transferred to HPLC vials for LC-MS/MS analysis.

2.2.2 LC-MS/MS analysis

Intracellular and extracellular concentrations of DON, DON-3-Sulf, DON-15-Sulf were determined by LC-MS/MS analysis using an established MRM method (Warth et al. 2016). In brief, the analysis was performed on an UltiMate 3000 UHPLC system connected to a TSQ Vantage triple quadrupole mass spectrometer equipped with a heated electrospray ionization interface (Thermo Fisher Scientific, Germany). A Kinetex Biphenyl 100Å LC column (C18, 2.6µm, 150 cm x 3 mm) and an optimized elution gradient (Eluent A – 10% MeOH in water + 0.05% HAc; Eluent B - MeOH + 0.05% HAc) were utilized to achieve chromatographic separation of isomers. The mass spectrometer was operated in negative ionization mode performing multiple reaction monitoring (MRM). The following transitions were monitored: DON *m/z* 355 $[M+Ac]^-$ →265/247; DON-15-Sulf m/z 375 $[M-H]^-$ → 97/163; DON-3-Sulf m/z 375 $[M-H]^-$ →345/97. Xcalibur software 3.0 (Thermo Fisher Scientific, Germany) was used to operate the system and TraceFinder 3.3 (Thermo Fisher Scientific, Germany) to evaluate the data. To account for matrix effects during the electrospray ionization process (Schwartz-Zimmermann et al. 2015; Warth et al. 2016), cell lysates and supernatants were spiked with a multi-standard stock solution and all results corrected for the apparent recovery.

2.3. *In silico* modelling experiments

The binding architectures within the ribosome binding site and the structure-activity relationship of DON and DON-sulfates have been analyzed *in silico* using a validated molecular model relying on docking simulations and rescoring procedures (Dellafiora et al. 2017). Such an integrated procedure proved to be reliable in assessing the toxicity of low-molecular weight molecules and estimating semi-quantitatively the interaction of ligands within targets' ligand binding pocket (Cozzini and Dellafiora 2012; Dellafiora et al. 2015; Ehrlich et al. 2015). The efficacy in assessing the interaction of trichothecenes with the ribosome toxin site has been additionally proved (Dellafiora et al. 2017). Therefore, assessing the capability of DON and DON-sulfates to fit the ribosome binding site has been used herein to infer the structural rationale at the basis of the different ribotoxic activity found experimentally.

In more detail, the 3D model for the ribosome was derived from the Protein Data Bank (http://www.rcsb.org) structure having PDB code 4U53 (Garreau de Loubresse et al. 2014). The ribosome structure and ligands were processed according to Dellafiora and co-workers (Dellafiora et al. 2017) using the software Sybyl, version 8.1 (www.certara.com). All atoms were checked for atom- and bond-type assignments. Amino- and carboxyl-terminal groups were set as protonated and deprotonated, respectively. Hydrogen atoms were computationally added to the protein and energy-minimized using the Powell algorithm with a coverage gradient of $\leq$ 0.5 kcal (mol Å)$^{-1}$ and a maximum of 1500 cycles.

The toxin binding site was defined by using the Flapsite tool of the FLAP (Fingerprint for Ligand And Protein) software (Molecular Discovery Ltd; http://www.moldiscovery.com) (Baroni et al. 2007), while the corresponding pharmacophoric space was investigated by using the GRID algorithm (Carosati et al. 2004). Specifically, the DRY probe was used to describe the hydrophobic environment, while the sp2 carbonyl oxygen (O) and the neutral flat amino (N1) probes were used to describe the hydrogen bond acceptor and donor capacity of the pocket, respectively.

Docking simulations were performed using the program GOLD version 5.2 (CCDC; Cambridge, UK; http://www.ccd.cam.ac.uk) on a double-quad cores machine equipped with 1.86 GHz processors. The

workflow and software setting reported by Dellafiora (Dellafiora et al. 2017) were used. In brief, the ribosome has been kept semi-rigid (only polar hydrogen atoms were set freely to rotate), while ligands were set fully flexible. For each ligand, 100 poses were generated and all of them were rescored with the DSX scoring function (Neudert and Klebe 2011). Only the best scored pose for each compound was kept. Notably, the lower the score, the better the interaction as DSX function estimates the thermodynamic stability of intermolecular interactions. Additionally, GOLD implements a Lamarckian genetic algorithm that may introduce variability in the results. Therefore, all the analyses were done in triplicate to exclude score differences due by chance. The mean values ± standard deviation (SD) are reported. Statistical analysis of computational results was done using IBM SPSS Statistics for Windows, version 19 (IBM Corp., Armonk, NY). Data were statistically analyzed by one-way ANOVA ($\alpha = 0.05$), followed by post hoc Fisher's least significant difference (LSD) test ($\alpha = 0.05$). All images were obtained using the software PyMol version 1.7 (http://www.pymol.org).

2.4. Intracellular level of reactive oxygen species (ROS)

For the measurement of the intracellular ROS, cells were pre-incubated with 50 µM of DCFH-DA (100 µl, 30 min, 37 °C). Afterwards, DCFH-DA containing solution was discarded, cells were rinsed with PBS and a first measurement of fluorescence was performed (ex./em. 480 nm/520 nm). Measurements were carried out in phenol red-free DMEM (Gibco; 10 % FCS, 1 % P/S, 25 mM HEPES) with different concentrations of DON, DON-3-Sulf, DON-15-Sulf and 1 % H_2O (negative control) or hydrogen peroxide (H_2O_2 500 µM, positive control). Fluorescence values were acquired after 5, 10, 30, 60, 90, 120 and 180 min of incubation with a multi-mode microplate reader Cytation3 Imaging Multi-Mode Reader (BioTek, Winooski, VT, USA). Of the experiments at least five independent biological replicates were performed in hexuplicates. Data are presented as the means ± standard error of the mean (S.E.M.) and the statistical analysis was performed with Origin Pro 9.1G (OriginLab, Northampton, USA). For all the calculations statistical levels are set to 5 % and the normal distribution of the data was tested using the Shapiro Wilk test. Statistical evaluation of the concentration series of single substances was

conducted using the one-way analysis of variance (ANOVA) and in case of a significant difference ($p < 0.05$) post-hoc Fisher's least significant difference (LSD) test was used.

2.5. Effect on gene transcription

The potential effect of DON-3-Sulf and DON-15-Sulf to modulate the transcription of genes involved in redox homeostasis and cell protection was tested by quantitative real-time PCR (qPCR). Total RNA was extracted (RNeasy®Mini Prep Kit, Qiagen Hilden, Germany) and reverse transcribed into complementary DNA (cDNA; QuantiTect® Reverse Transcription Kit, Qiagen, Hilden, Germany) following the supplier's protocols. Complementary DNA was amplified in duplicates in the presence of QuantiTect® SYBR® Green Master Mix (Qiagen) and gene specific primers (QuantiTect® Primer Assays, Qiagen) with the StepOnePlus™ System (Applied Biosystems). Following QuantiTect® Primer Assays were used: β-actin (Hs_ACTB1_1_SG, QT00095431), glyceraldehyde 3-phosphate dehydrogenase (GAPDH, Hs_GAPDH_2_SG, QT01192646), kelch-like ECH-associated protein 1 (Keap-1, Hs_KEAP1_1_SG, QT00080220), nuclear factor (erythroid-derived 2)-like 2 (Nrf-2, Hs_NFE2L2_1_SG, QT00027384) gamma-glutamate-cysteine ligase (Hs_GCLC_1_SG, QT00037310), NAD(P)H dehydrogenase quinine 1 (NQO-1, Hs_NQO1_1_SG, QT00050281) and interleukin 8 (IL-8, Hs_CXCL8_1_SG, QT00000322), cyclooxygenase 2 (Cox-2, Hs_PTGS2_1_SG, QT00040586). A universal PCR protocol was applied (enzyme activation: 15 min at 95 °C; 40 cycles of 15 sec at 94 °C, 30 sec of 55 °C and 30 sec at 72 °C). The StepOnePlus® software v2.1 was used for analysis and quantitation of fluorescence signals. At least three independent experiments were performed. Gene transcription is presented as relative amount of transcripts normalized to the mean of transcript levels of endogenous control genes (ACTB1, GAPDH) applying the ΔΔCt-method as PCR efficiencies of target and control genes have been found comparable. The results are plotted as mean ± (SEM). Origin 9.1.0G software was used for graphical and statistical analysis. Significances are calculated with independent one-way ANOVA and Fisher LSD post hoc test after passing the test for normal distribution of the data.

2.6. Cytotoxic potential of DON-3-Sulf and DON-15-Sulf in comparison to DON

2.6.1 WST-1 assay

After 24 h of incubation with DON, DON-3-Sulf and DON-15-Sulf (concentration range 1 nM-10 µM), cell viability/proliferation was measured with the cell proliferation reagent WST-1 (Roche Diagnostics GmbH, Mannheim, Germany). The reagent was diluted 1:10 (v/v) in serum free DMEM medium and applied to HT-29 cells for 35 minutes. Subsequently, absorbance was measured at 450 nm with reference wavelength at 650 nm using a Cytation3 Imaging Multi-Mode Reader (BioTek, Winooski, VT, USA). At least five independent biological replicates were performed, each in quadruplicate. WST-1 data are presented as the means ± SEM and their statistical analysis was performed with Origin Pro 9.1G software. For all the calculations statistical levels are set to 5 % and the normal distribution of the data was tested using the Shapiro Wilk test. Statistical evaluation of the concentration series of the single substances was conducted using the one-way analysis of variance (ANOVA) and in case of a significant difference ($p < 0.05$) the post-hoc Fisher's least significant difference (LSD) test was used.

2.6.2. Measurement of cell density/ confluence

Brightfield images were acquired for the evaluation of the confluence reached by the cells in the wells after the incubation with DON or the metabolites in comparison to non-treated controls. Subsequently, cells were rinsed with PBS and medium was replaced by Life Cell Imaging solution (Thermo Fisher Scientific). Imaging of the complete well surface was obtained with a 3x4 image montage of the Cytation3 Imaging Multi-Mode Reader (BioTek, Winooski, VT, USA). Digital phase contrast processing was applied to the images using BioTek Gen5 software version 2.09.2. (BioTek, Winooski, VT, USA). Afterwards, the threshold was identified for each optical field and confluence was calculated with the image statistic mode. Of the experiments, at least three independent biological replicates were performed in quadruplicates. Cellular confluence data are presented as the means ± SEM and their statistical analysis was performed with Origin Pro 9.1G. For all the calculations statistical levels are set to 5 % and the normal distribution of the data was tested using the Shapiro Wilk test. Statistical evaluation of the concentration series of single substances was conducted using the one-way analysis of variance (ANOVA) and in case of a significant difference ($p < 0.05$) the post-hoc

Fisher's least significant difference (LSD) test was used. If less than five independent biological replicates were performed of an experiment a non-parametric method, namely the Kruskal-Wallis ANOVA, was applied.

2.7. Immunocytochemistry

For immunofluorescence experiments, cells were incubated according to the respective experimental design, rinsed with pre-warmed PBS and fixed with formaldehyde (3.7 % in PBS, 20 min). Permeabilization was performed with Triton-X (0.2 % in PBS) and blocking with 1 % of BSA in PBS (1 h, RT; Ki-67 determination) or 2 % of donkey serum (LC3 determination). Afterwards, cells were incubated with primary antibodies (Ki-67 antibody sc-15402; anti α-Tubulin antibody sc-5286, anti Lamin-B antibody sc-6216 from Santa Cruz Biotechnology, Dallas US; anti LC3B antibody from Thermo Fisher Scientific, Waltham US) for 2 h (RT). Cells were rinsed with washing buffer (0.01 % of Triton in PBS) and incubated for 1.5 h with fluorescent labeled secondary antibodies (Donkey anti goat IgG Alexa Fluor 647, Donkey anti mouse IgG Alexa Fluor 488, Donkey anti rabbit IgG Alexa Fluor 568 all from Thermofisher Scientific, Waltham US). At the end of the staining unbound antibodies were removed through several washing steps and the samples were post fixed (3.7 % of formaldehyde in PBS, 10 min, RT) and, ultimately reactive sites were masked with 100 mM of glycine (5 min, RT). Slides were mounted with ProLong Diamond Antifade Mountant with or without DAPI, according to the experimental need (Thermo Fisher Scientific, Waltham US). Images were acquired with LSM Zeiss 710 equipped with ELYRA PS.1 system with a Plan Apochromat 63X/1.4 oil objective (zoom 1.5) and an AndoriXon 897 (EMCCD) camera. Images were analyzed with ZEN 2012 SP3 (black). For the quantification of the intensity of Ki-67 maximum intensity projection of the images were obtained from the total signal included in the 3D reconstructions and intensity of the signal was calculated after background correction. For the quantification of the cells in active mitosis images were acquired with a Plan Apochromat 10X objective and images were quantified offline expressing % of cells actively replicating as ratio between cells with condensed mitotic spindle and total cell number per optical field (mitotic index / optical field). SIM images were obtained with a Plan Apochromat 100X (1.46 NA)

objective. Data analysis was performed using Microsoft Excel 2013. Of the experiments, at least four independent biological replicates were performed in triplicates. KI-67 quantification data are presented as the means ± SEM and their statistical analysis was performed with Origin Pro 9.1G. For all the calculations statistical levels are set to 5 % and the normal distribution of the data was tested using the Shapiro Wilk test. Statistical evaluation of the concentration series of single substances was conducted using the one-way analysis of variance (ANOVA) and in case of a significant difference ($p < 0.05$) the post-hoc Fisher's least significant difference (LSD) test was used. If less than five independent biological replicates were performed of an experiment a non-parametric method, namely the Kruskal-Wallis ANOVA, was applied.

3. Results

3.1. Evaluation of cellular uptake of DON and its sulfate conjugates by LC-MS/MS

To investigate if the apparent lack of toxicity of DON-3-Sulf and DON-15-Sulf in HT-29 (Warth et al. 2016) could be due to a reduced absorption of the compounds at cellular level, uptake experiments were performed.

DON and its sulfates were quantified in the cell extracts (Figure 1A) and, sulfate conjugates that have been taken up by the cells were found, although at lower levels compared to DON. DON, which might be generated by hydrolysis of the sulfates, was not detected in the cell extracts after incubation with DON-3-Sulf or DON-15-Sulf. No significant difference between the two DON-sulfates was apparent with respect to cellular uptake. In the cell culture medium the DON-sulfates were retrieved at a slightly higher concentration compared to DON (Figure 1B). All three compounds proved to be stable in the culture medium for at least 24 h (Figure 1B, C).

3.2. *In silico* modelling of the structural basis of the different ribotoxicity of DON and sulfate conjugates

According to previous studies (Pierron et al. 2016), DON fits the ribosome A-site engaging the surrounding environment with three polar interactions, one with the Mg^{2+} ion forming the binding site. In the present work (Figure 2), the interaction of DON-3-Sulf and DON-15-Sulf with the ribosome A-site has been calculated and compared to that of DON to define the molecular mechanisms sustaining the difference in toxicity. DON-3-Sulf and DON-15-Sulf scores were less negative in comparison to DON ($p < 0.001$ and 0.01, respectively), albeit maintaining the same binding orientation, indicating a poor fit in the toxin binding site. In more detail, DON-3-Sulf interaction was found impaired by an evident sterical interference with the Mg^{2+} ion, causing an extensive score worsening. DON-15-Sulf recorded a smaller reduction of the score, indicating a mismatch with these pharmacophores. Indeed, the sulfate group was found improperly arranged within a space suitable for receiving hydrophobic groups causing hydrophobic/polar interferences.

3.3. DON and its sulfated forms differ in their potency to induce a rapid cellular oxidative stress response

DON is known to impact oxidative stress on HT-29 cells (Krishnaswamy et al. 2010), experiments were performed to test the potential of DON-3-Sulf and DON-15-Sulf to trigger a similar mechanism. DON triggered a fast and concentration dependent increase of ROS in HT-29 cells (measured as DCFH-DA experiments), detectable at a concentration of 10 µM (Figure 3A). Similarly, 10 µM DON-3-Sulf induced a significant increase in comparison to control cells within the first 3 min of the application of the toxin (Figure 3A). Although the amplitude of the response did not reach the one elicited by the positive control (500 µM H_2O_2), it remained appreciable in comparison to controls for approximately 1 h. In fact, the values of intracellular ROS remained elevated up to 60 min after the addition of the toxin to the extracellular medium (Figure 3A-D). Similarly, after 1 h of incubation, DON-3-Sulf triggered a transient response even at the very low concentrations of 0.1 and 1 µM and DON-15-Sulf at 1 µM (Figure 3D).

3.4. Impact of DON and DON-sulfates on transcription of genes governing oxidative stress and inflammatory response

DON has the potential to induce signaling pathways related to the cellular antioxidant response (Katika et al. 2015) and intestinal inflammation (Krishnaswamy et al. 2010). In line with previous data (Katika et al. 2015), the effect of DON on Nrf2/ARE dependent genes was mirrored by the moderate increase of Nrf2 transcript levels in HT-29 cells. After 3 h of incubation, a significant and concentration-dependent increase of mRNA was observed (1 and 10 µM, Fig. 4A). However the benchmark of a two-fold change was not achieved. In parallel, a decrease of transcription of Keap-1 gene was detected in cells incubated with the highest concentration of DON (Fig. 4B). This effect measured after 3 h incubation was still persistent after a longer incubation time (24 h, 10 µM DON; supplementary material S1). From the group of genes known to possess an antioxidant response element (Nrf2-binding site) in their promoter, γGCL (gamma- glutamate-cysteine ligase) and NQO1 (NAD(P)H quinone dehydrogenase 1) were selected. The transcript level of γGCL was marginally increased upon exposure

to 1 µM DON, yet with statistical significance (Fig. 4D), whereas NQO-1 transcription was found to be suppressed statistically significant at 10 µM DON. (Fig. 4C). Short time incubation (3 h) with DON-3-Sulf at a concentration ≥1 µM resulted in a concentration dependent decrease of Nrf-2, Keap-1 and NQO-1 transcription, however statistical significant only for Keap-1 at 10 µM (Fig. 4B). DON-15-Sulf (0.1 µM) triggered a transient increase of NQO-1 transcripts after 3 h incubation. In agreement with the literature, the mRNA levels of pro-inflammatory cytokine IL-8 and cyclooxygenase-2 (COX-2) were potently increased by DON (1 µM and 10 µM) in HT-29 colon cells (Fig. 4E, F). In contrast, the two sulfated DON-metabolites had no impact on IL-8 and COX-2 transcription, indicating that pro-inflammatory effects potentially are not to be expected for both metabolites.

3.4. Effect of DON and DON-sulfates on proliferation of HT-29 cells

It was previously demonstrated that DON-3-Sulf and DON-15-Sulf have the potential to increase the proliferation of cancer cells, namely increasing the total cellular protein content (sulforhodamine B assay, (Warth et al. 2016)). In the present study, the cytotoxic potential of the DON sulfates was measured via WST-1 and with the confluence analysis. Measurement of mitochondrial activity after incubation with DON-3-Sulf and DON-15-Sulf (WST-1 assay, Figure 5A) showed a tendency to decrease the metabolism of the WST-1 dye at concentrations inferior to 0.1 µM and to increase it at higher concentrations. Confluency analysis revealed that cells treated with the sulfated DONs tended to be more confluent than DON-treated cells (concentrations > 1 µM), although a statistically significant difference relative to DON was found only for 1 µM DON-3-Sulf (Figure 5B). A specific biomarker of proliferation, Ki67 was used as previously described (Wittig et al. 2017), to confirm the effect of DON-3-Sulf and DON-15-Sulf on HT-29 cells (Figure 6). Quantification of the fluorescent signal revealed a significant increase of Ki67 in cells incubated with the DON-15-Sulf and DON-3-Sulf (0.1 µM). In agreement with the cytotoxicity assays, 10 µM DON triggered a significant decrease of the Ki67 signal. Quantification of the cells with visible mitotic spindle, indicating active duplication, was performed. In line with previous results, incubation with 0.1 µM of DON-15-Sulf increased the number of actively replicating cells in comparison to control cells. Cells incubated with DON-3-Sulf and DON-15-Sulf (10

μM) presented higher number of cells in mitosis in comparison the parent compound DON (quantified as % of cells duplicating/total number of cells optical field, Figure 7).

3.5. Effect of DON-sulfates on cellular autophagy

In the frame of the regulation of cellular homeostasis, autophagy plays a central role in discriminating between proliferation and cell response to stressors (Kroemer et al. 2010). Since DON-sulfates proved to be effective in triggering HT-29 proliferation, the activity of the compounds with respect to autophagy was tested. To this aim, LC3 protein (Han et al. 2016) was chosen as one of the key elements for the assembly of the nascent autophagosomes (Kroemer et al. 2010) and, consequently, one of the most used biomarkers of the processes. In cells incubated with 0.1 μM of DON, DON-3-Sulf and DON-15-Sulf a clear increase of the LC-3 signal determined by immunolocalization was observed, suggesting the activation of the autophagic machinery, in particular in cells undergoing mitosis. For DON-3-Sulf and DON-15-Sulf the effect was even more visible in cells incubated with the highest concentration of the compounds. In cells incubated with 10 μM of DON a diffuse increase of the signal of LC3 was observed. Moreover, SIM imaging allowed the visualization at high resolution of the relation between LC3 accumulation and the mitotic spindle (Figure 8 white arrows).

4. Discussion

With the increase of the sensitivity of analytical methods, a rising number of mycotoxins and their metabolic products is discovered. Hence, the need to comprehend the toxicological potential of such new modified forms is a renewing priority. Sulfate derivatives have been discovered for several relevant mycotoxins. This includes sulfated metabolites of *Alternaria* mycotoxins (Soukup et al. 2016; Walravens et al. 2016), as well as metabolites of compounds produced by *Fusarium* spp. (Binder et al. 2017). Deoxynivalenol is no exception, and it was recently detected in modified forms, conjugated with sulfate moieties in positions C-3 (DON-3-Sulf) and C-15 (DON-15-Sulf) (Fruhmann et al. 2014a; Schwartz-Zimmermann et al. 2015; Wan et al. 2014; Warth et al. 2016; Warth et al. 2015). In spite of structural characterization of these compounds, comparatively little is known about their molecular targets and mechanism of action (Payros et al. 2016). Chronic low dose exposures towards DON and its congeners/metabolites have been reported in several populations via biomonitoring surveys (Sarkanj et al. 2013; Solfrizzo et al. 2014; Turner et al. 2008; Warth et al. 2014; Warth et al. 2012) and still represent an open challenge in the risk assessment of DON (Alizadeh et al. 2016; Dellafiora and Dall'Asta 2017).

It was previously demonstrated that DON-3-Sulf and DON-15-Sulf lack the classic cytotoxic effect of DON by inhibition of protein translation (Warth et al. 2016). Considering the increased polarity of the modified forms, it could not be excluded that the conjugation with the sulfate moiety might reduce their absorption through membranes, thus explaining, at least partially, the loss of toxicity. As demonstrated in Figure 1, DON-3-Sulf and DON-15-Sulf were recovered in the intracellular compartment after an incubation time of 24h, thus strongly suggesting their uptake at the intestinal level. However, in line with the expected chemical behavior related to sulfation, i.e. increased polarity, the concentration of the two metabolites in the intracellular compartment was lower than that of DON. Li and co-workers (Li et al. 2017) recently described the efflux of DON from intestinal cells to be mediated primarily by organic anion transporting peptides. Accordingly, it might be speculated that

sulfate conjugation also increases the affinity of DON-metabolites for this mechanism, possibly promoting their extrusion from the cells.

Once ascertained that DON-sulfates are taken up by cells, *in silico* experiments were performed to better describe the interaction of the metabolites with the ribosome. Trichothecenes inhibit protein synthesis interacting with the A-site of the major ribosome subunit, thereby impairing the arrangement of tRNAs in the peptidyl transferase center (Garreau de Loubresse et al. 2014; Payros et al. 2016). It was previously reported that DON-sulfates have a reduced capability to inhibit protein synthesis *via* ribosome inactivation in comparison to DON (Warth et al. 2016), and reduced interaction of DON-sulfates with the proposed trichothecene binding site has been hypothesized as a possible explanation (Dellafiora et al. 2017). In the present work, the interaction of DON and DON-sulfates within the ribosome A-site was analyzed in detail using a molecular modelling approach. The *in silico* model used was able to predict the observed effects of DON on translation (Warth et al. 2016; Warth et al. 2015), supporting its reliability in predicting the binding modes of sulfate conjugates too. Noticeably, the ranking of the *in silico* binding scores was consistent with the protein synthesis inhibitory activity found *in vitro*; in fact, no activity was seen for DON-3-Sulf up to 100 µM and DON-15-Sulf showed only a limited effect when compared to DON (Warth et al. 2016; Warth et al. 2015). Therefore, despite the relatively minor structural modifications, the three compounds differ substantially in the capability to interact within the ribosome. However, the outcome of the binding of the DON-sulfates at ribosomal level did not completely explain the lack of cytotoxicity of DON-15-Sulf or the potential of DON-3-Sulf and DON-15-Sulf to increase cellular proliferation. Reactive Oxygen Species (ROS) production is commonly a very fast cellular response to toxicants but, in appropriate conditions, it can also stimulate cellular proliferation (Sciancalepore et al. 2012). It was previously demonstrated that DON can trigger the increase of ROS as one of the mechanisms sustaining its cytotoxic potential (Wu et al. 2014). In HT-29 cells DON and DON-sulfates triggered a fast and transient increase of intracellular ROS (Figure 3). This effect, despite being concentration dependent within the first 10 min post-exposure (Figure 3A and B), extinguished almost completely within 60 minutes from

the beginning of the incubation (Figure 3D). Interestingly, the kinetic of the oxidative stress response triggered by DON and DON-sulfates differed substantially from that of H_2O_2, suggesting the initial effect of the toxins to be buffered by intracellular responses, or more likely a direct effect rather unable to trigger a sustained response, which would be more likely for H_2O_2. Moreover, the effect of DON and derivatives on ROS was detectable almost exclusively at concentration ≥ 1 µM. As confirmed also in this study (Figures 5-7), the most prominent effect on proliferation mediated by trichothecene mycotoxins is observed in the sub-micromolar concentration range (Manda et al. 2015; Warth et al. 2016). In this light, the involvement of the oxidative stress in sustaining DON-mediated cellular proliferation seemed unlikely. Moreover, the very limited mitochondrial impairment measured in the WST-1 assay (Figure 5A), sustains the interpretation that DON and DON-sulfates might have a negligible impact on ROS homeostasis in HT-29 cells. In parallel, the incubation of HT-29 cells with DON also triggered a significant increase of the relative gene transcription of Nrf2. Nrf2 is one of the key elements governing the antioxidant response in cells, thus playing an essential role in ensuring protection from toxicants (Jarolim et al. 2017; Jiang et al. 2009; Wang et al. 2007). However, the effect of DON on the transcription of the genes regulated by the Nrf2/ARE-pathway in HT-29 was minor and very limited, implying a potential inducing effect only on the gene transcription of Nrf2 (1 µM and 10 µM DON) and γGCL (1 µM DON). Whether the statistically significant increase of transcript levels, which is still below the in general accepted two-fold increase, is of biological relevance remains open. In addition, since pro-inflammatory potential is one of the main features of DON-mediated toxicity (Pestka 2010a), relevant pro-inflammatory targets were included in the qPCR experiments. In agreement with the literature, DON triggered the increase of the gene transcription of the pro-inflammatory mediators IL-8 and COX-2 (Figure 4E, F). However, as previously discussed in the context of oxidative stress, the effect of DON on pro-inflammatory mediators occurred only at concentrations ≥ 1 µM and was not observed for DON-3-Sulf and DON-15-Sulf, ruling out the possibility that inflammatory effects could play a role in sustaining the proliferative stimulus of the two metabolites. In agreement with previous studies (Wittig et al. 2017), Ki-67 was used as a marker of proliferation in HT-29 cells. Quantification of the signal associated to the immunolocalization of Ki-67 revealed an

increase in cells incubated with 0.1 µM of DON-3-Sulf and DON-15-Sulf (Figure 6). In parallel, the quantification of the cells with visible mitotic spindles confirmed an increase of the cells actively duplicating (Figure 7). This effect was particularly prominent for DON-15-Sulf. It was previously demonstrated that NQO-1 tends to localize at the mitotic spindle level in human cells (Siegel et al. 2012) and, interestingly, its gene transcription in cells incubated with DON-15-Sulf showed a tendency toward increase (Figure 4C). Concomitantly, 10 µM of DON inhibited both the formation of the mitotic spindles and expression of Ki-67, which is in agreement with its cytotoxic potential, as well as with the inhibition of the protein synthesis (Warth et al. 2016). Effect of DON-sulfates on HT-29 proliferation was confirmed with metabolic assays, biochemical markers as wells as with the measurements of the mitotic spindle and cell confluency (Figures 5-7). This combination of assays reduced the chance that the increase of the signal (proliferation) could be an artifact related to altered cell metabolism and pointed to an increase of cell number.

Cellular proliferation is tightly regulated by nutrients supplies, as well as from the availability of biochemical “building blocks” necessary for cell growth. In this respect, autophagy plays a central role in ensuring the efficient recycling of cellular components and regulating their availability (Kroemer et al. 2010). Moreover, it is well-known that autophagy plays a key role in regulating protein turnover (Vlada et al. 2015) and it is essential during mitosis in order to ensure the clearance of damaged mitochondria during the duplication (Liu et al. 2009). In order to verify the effect of DON and metabolites on the autophagic pathway, immunolocalization experiments of the LC3 protein were performed. Interestingly, the signal of the autophagy biomarker (Han et al. 2016; Solhaug et al. 2014), increased in cells incubated with 0.1 µM of DON and DON-sulfates (Figure 8), whereas in cells incubated with 10 µM of DON presented a diffuse pattern of LC3 localization. Controlled autophagy represents a protective mechanism against the toxicity of DON, thus increasing the clearance of damaged proteins-organelles and reducing cell stress (Tang et al. 2015). The hypothesis of a sustained activation of the autophagic pathway upon incubation with low concentration of DON and DON-sulfates matches the effects of the compounds on the WST-1 assay. In this respect, enhanced

mitochondrial turnover (Kulikov et al. 2017; Malena et al. 2016), thus more efficient elimination of the organelles, could account for transient decrease of the capability of the cells to metabolize the WST-1 reagent resulting, as shown in Figure 5 in a transient decrease of the signal at sub-toxic concentrations. It was recently suggested that sulfate metabolites can have a marked affinity for the lysosomal compartment. In fact, using resveratrol-sulfates as model, Andreadi and colleagues proposed the accumulation of the sulfate derivatives in the acidic organelles, followed by a low release of the parent compound due to the action of lysosomal sulfatases (Andreadi et al. 2014; Frankel et al. 2014). Hypothesizing that DON-3-Sulf and DON-15-Sulf could share a similar behavior, the release/generation of the parent compound DON in the intracellular compartment could be a very slow process. In agreement with this interpretation, the equilibrium concentration of DON in the cell lysate could be below the detection limit of the LC-MS/MS method. In this light, it would be possible to justify the apparent lack of parent compound DON in the cells incubated with DON-3-Sulf and DON-15-Sulf observed in the LC-MS/MS experiments. Combining the results of the *in silico* modelling together with the effect of the three molecules on the autophagic pathway, we propose at least three possible differential mechanisms of interplay between ribosomal inhibition and autophagy as outlined in Figure 8. In more general terms, DON possesses the highest affinity for the ribosome promoting the block of protein synthesis. If this event is limited, (i.e. at low concentrations as 0.1 µM DON), the accumulation of damaged proteins could be handled by the cells through the activation of controlled autophagy. This event would provide building blocks necessary to the cells to stimulate limited proliferation, as previously reported (Manda et al. 2015; Warth et al. 2016). On the other hand, according to the data provided by *in silico* modelling (Figure 2 and (Dellafiora et al. 2017)) and the ribosomal inhibition assay (Warth et al. 2016; Warth et al. 2015), the affinity of DON-3-Sulf for the ribosome is negligible. This might favor the direct transport of the molecule toward the lysosomal compartment, followed by release of parent DON in low amounts (as similarly described in (Andreadi et al. 2014)), and eventually causing partial ribosomal inhibition, as described for low concentrations of DON. DON-15-Sulf showed a limited affinity to the ribosomal pocket and a potent effect on the autophagal machinery suggesting an intermediate behavior in comparison to DON and DON-3-Sulf. Moreover, for all three compounds

the possibility to form Michael adducts with SH groups might be considered, as shown for small molecules such as glutathione (Fruhmann et al. 2014b), sulfite (Schwartz et al. 2013) and also free cysteine (Stanic et al. 2016). It is long known that type B trichothecenes can also inhibit the activity of enzymes with thiol functionality, such as lactate dehydrogenase and alcohol dehydrogenase (Ueno and Matsumoto 1975). Formation of thiol-adducts with proteins could be an explanation for the inability to detect free DON, and potentially such adducts might be also degraded in the lysosome. In conclusion, we propose that DON-sulfates activate intracellular pathways alternative and complementary to the classical ribosomal inhibition typical for trichothecene mycotoxins and provide a mechanistic explanation towards the proliferative effects of DON-sulfates in HT-29 cells.

Conflict of Interest

None Declared.

Acknowledgments

The authors are grateful to Mrs. Eva Attakpah for careful technical assistance and to Dr. Philipp Fruhmann for the availability of the DON-sulfates. LC-MS/MS measurements were performed at the Mass Spectrometry Center of the Faculty of Chemistry of the University of Vienna.

The authors thank the Austrian Science Fund for support (project SFB Fusarium #F3718, and F3702).

Author contributions:

GDF, LW, DB, HP, MLK, LD, BW, GP performed the experiments and analyzed the data. GDF, GA, BW, CD and DM planned the experiments and interpreted the results. All the authors contributed to the integration of the research and to the preparation of the manuscript.

References

Alizadeh A, Braber S, Akbari P, Kraneveld A, Garssen J, Fink-Gremmels J (2016) Deoxynivalenol and Its Modified Forms: Are There Major Differences? Toxins 8(11) doi:10.3390/toxins8110334

Andreadi C, Britton RG, Patel KR, Brown K (2014) Resveratrol-sulfates provide an intracellular reservoir for generation of parent resveratrol, which induces autophagy in cancer cells. Autophagy 10(3):524-5 doi:10.4161/auto.27593

Baroni M, Cruciani G, Sciabola S, Perruccio F, Mason JS (2007) A common reference framework for analyzing/comparing proteins and ligands. Fingerprints for Ligands and Proteins (FLAP): theory and application. Journal of chemical information and modeling 47(2):279-94 doi:10.1021/ci600253e

Bhat RV, Beedu SR, Ramakrishna Y, Munshi KL (1989) Outbreak of trichothecene mycotoxicosis associated with consumption of mould-damaged wheat production in Kashmir Valley, India. Lancet (London, England) 1(8628):35-7

Binder SB, Schwartz-Zimmermann HE, Varga E, et al. (2017) Metabolism of Zearalenone and Its Major Modified Forms in Pigs. Toxins 9(2) doi:10.3390/toxins9020056

Carosati E, Sciabola S, Cruciani G (2004) Hydrogen bonding interactions of covalently bonded fluorine atoms: from crystallographic data to a new angular function in the GRID force field. Journal of medicinal chemistry 47(21):5114-25 doi:10.1021/jm0498349

Cozzini P, Dellafiora L (2012) In silico approach to evaluate molecular interaction between mycotoxins and the estrogen receptors ligand binding domain: a case study on zearalenone and its metabolites. Toxicology letters 214(1):81-5 doi:10.1016/j.toxlet.2012.07.023

Cundliffe E, Cannon M, Davies J (1974) Mechanism of inhibition of eukaryotic protein synthesis by trichothecene fungal toxins. Proceedings of the National Academy of Sciences of the United States of America 71(1):30-4

Danicke S, Brezina U (2013) Kinetics and metabolism of the Fusarium toxin deoxynivalenol in farm animals: consequences for diagnosis of exposure and intoxication and carry over. Food and chemical toxicology : an international journal published for the British Industrial Biological Research Association 60:58-75 doi:10.1016/j.fct.2013.07.017

Dellafiora L, Dall'Asta C (2017) Forthcoming Challenges in Mycotoxins Toxicology Research for Safer Food-A Need for Multi-Omics Approach. Toxins 9(1) doi:10.3390/toxins9010018

Dellafiora L, Dall'Asta C, Cruciani G, Galaverna G, Cozzini P (2015) Molecular modelling approach to evaluate poisoning of topoisomerase I by alternariol derivatives. Food chemistry 189:93-101 doi:10.1016/j.foodchem.2015.02.083

Dellafiora L, Galaverna G, Dall'Asta C (2017) In silico analysis sheds light on the structural basis underlying the ribotoxicity of trichothecenes-A tool for supporting the hazard identification process. Toxicology letters doi:10.1016/j.toxlet.2017.02.015

Ehrlich VA, Dellafiora L, Mollergues J, et al. (2015) Hazard assessment through hybrid in vitro / in silico approach: The case of zearalenone. Altex 32(4):275-86 doi:10.14573/altex.1412232

European Food Safety A (2013) Deoxynivalenol in food and feed: occurrence and exposure. EFSA Journal 11(10):3379-n/a doi:10.2903/j.efsa.2013.3379

Frankel LB, Di Malta C, Wen J, Eskelinen EL, Ballabio A, Lund AH (2014) A non-conserved miRNA regulates lysosomal function and impacts on a human lysosomal storage disorder. Nature communications 5:5840 doi:10.1038/ncomms6840

Fruhmann P, Skrinjar P, Weber J, et al. (2014a) Sulfation of deoxynivalenol, its acetylated derivatives, and T2-toxin. Tetrahedron 70(34):5260-5266 doi:10.1016/j.tet.2014.05.064

Fruhmann P, Weigl-Pollack T, Mikula H, et al. (2014b) Methylthiodeoxynivalenol (MTD): insight into the chemistry, structure and toxicity of thia-Michael adducts of trichothecenes. Organic & biomolecular chemistry 12(28):5144-50 doi:10.1039/c4ob00458b

Garreau de Loubresse N, Prokhorova I, Holtkamp W, Rodnina MV, Yusupova G, Yusupov M (2014) Structural basis for the inhibition of the eukaryotic ribosome. Nature 513(7519):517-22 doi:10.1038/nature13737

Han J, Wang QC, Zhu CC, et al. (2016) Deoxynivalenol exposure induces autophagy/apoptosis and epigenetic modification changes during porcine oocyte maturation. Toxicology and applied pharmacology 300:70-6 doi:10.1016/j.taap.2016.03.006

Jarolim K, Del Favero G, Pahlke G, et al. (2017) Activation of the Nrf2-ARE pathway by the Alternaria alternata mycotoxins altertoxin I and II. Archives of toxicology 91(1):203-216 doi:10.1007/s00204-016-1726-7

Jiang T, Huang Z, Chan JY, Zhang DD (2009) Nrf2 protects against As(III)-induced damage in mouse liver and bladder. Toxicology and applied pharmacology 240(1):8-14 doi:10.1016/j.taap.2009.06.010

Katika MR, Hendriksen PJ, van Loveren H, A ACMP (2015) Characterization of the modes of action of deoxynivalenol (DON) in the human Jurkat T-cell line. Journal of immunotoxicology 12(3):206-16 doi:10.3109/1547691x.2014.925995

Krishnaswamy R, Devaraj SN, Padma VV (2010) Lutein protects HT-29 cells against Deoxynivalenol-induced oxidative stress and apoptosis: Prevention of NF-κB nuclear localization and down regulation of NF-κB and Cyclo-Oxygenase – 2 expression. Free Radical Biology and Medicine 49(1):50-60 doi:http://dx.doi.org/10.1016/j.freeradbiomed.2010.03.016

Kroemer G, Mariño G, Levine B (2010) Autophagy and the Integrated Stress Response. Molecular Cell 40(2):280-293 doi:10.1016/j.molcel.2010.09.023

Kulikov AV, Luchkina EA, Gogvadze V, Zhivotovsky B (2017) Mitophagy: Link to cancer development and therapy. Biochem Biophys Res Commun 482(3):432-439 doi:10.1016/j.bbrc.2016.10.088

Li F, Jiang D, Zhou J, Chen J, Li W, Zheng F (2016) Mycotoxins in wheat flour and intake assessment in Shandong province of China. Food additives & contaminants Part B, Surveillance:1-6 doi:10.1080/19393210.2016.1154109

Li FQ, Luo XY, Yoshizawa T (1999) Mycotoxins (trichothecenes, zearalenone and fumonisins) in cereals associated with human red-mold intoxications stored since 1989 and 1991 in China. Natural toxins 7(3):93-7

Li X, Mu P, Wen J, Deng Y (2017) Carrier-Mediated and Energy-Dependent Uptake and Efflux of Deoxynivalenol in Mammalian Cells. Scientific reports 7(1):5889 doi:10.1038/s41598-017-06199-8

Liu L, Xie R, Nguyen S, Ye M, McKeehan WL (2009) Robust autophagy/mitophagy persists during mitosis. Cell Cycle 8(10):1616-1620 doi:10.4161/cc.8.10.8577

Liu Y, Lu Y, Wang L, Chang F, Yang L (2016) Occurrence of deoxynivalenol in wheat, Hebei Province, China. Food chemistry 197 Pt B:1271-4 doi:10.1016/j.foodchem.2015.11.047

Malena A, Pantic B, Borgia D, et al. (2016) Mitochondrial quality control: Cell-type-dependent responses to pathological mutant mitochondrial DNA. Autophagy 12(11):2098-2112 doi:10.1080/15548627.2016.1226734

Manda G, Mocanu MA, Marin DE, Taranu I (2015) Dual effects exerted in vitro by micromolar concentrations of deoxynivalenol on undifferentiated caco-2 cells. Toxins 7(2):593-603 doi:10.3390/toxins7020593

Maul R, Warth B, Kant JS, et al. (2012) Investigation of the hepatic glucuronidation pattern of the Fusarium mycotoxin deoxynivalenol in various species. Chemical research in toxicology 25(12):2715-7 doi:10.1021/tx300348x

Neudert G, Klebe G (2011) DSX: a knowledge-based scoring function for the assessment of protein-ligand complexes. Journal of chemical information and modeling 51(10):2731-45 doi:10.1021/ci200274q

Payros D, Alassane-Kpembi I, Pierron A, Loiseau N, Pinton P, Oswald IP (2016) Toxicology of deoxynivalenol and its acetylated and modified forms. Archives of toxicology 90(12):2931-2957 doi:10.1007/s00204-016-1826-4

Pestka JJ (2010a) Deoxynivalenol-induced proinflammatory gene expression: mechanisms and pathological sequelae. Toxins 2(6):1300-17 doi:10.3390/toxins2061300

Pestka JJ (2010b) Deoxynivalenol: mechanisms of action, human exposure, and toxicological relevance. Archives of toxicology 84(9):663-79 doi:10.1007/s00204-010-0579-8

Pierron A, Mimoun S, Murate LS, et al. (2016) Microbial biotransformation of DON: molecular basis for reduced toxicity. Scientific reports 6:29105 doi:10.1038/srep29105

Pinton P, Oswald IP (2014) Effect of deoxynivalenol and other Type B trichothecenes on the intestine: a review. Toxins 6(5):1615-43 doi:10.3390/toxins6051615

Sarkanj B, Warth B, Uhlig S, et al. (2013) Urinary analysis reveals high deoxynivalenol exposure in pregnant women from Croatia. Food and chemical toxicology : an international journal published for the British Industrial Biological Research Association 62:231-7 doi:10.1016/j.fct.2013.08.043

Schmeitzl C, Warth B, Fruhmann P, et al. (2015) The Metabolic Fate of Deoxynivalenol and Its Acetylated Derivatives in a Wheat Suspension Culture: Identification and Detection of DON-15-O-Glucoside, 15-Acetyl-DON-3-O-Glucoside and 15-Acetyl-DON-3-Sulfate. Toxins 7(8):3112-26 doi:10.3390/toxins7083112

Schwartz-Zimmermann HE, Fruhmann P, Danicke S, et al. (2015) Metabolism of deoxynivalenol and deepoxy-deoxynivalenol in broiler chickens, pullets, roosters and turkeys. Toxins 7(11):4706-29 doi:10.3390/toxins7114706

Schwartz HE, Hametner C, Slavik V, et al. (2013) Characterization of three deoxynivalenol sulfonates formed by reaction of deoxynivalenol with sulfur reagents. Journal of agricultural and food chemistry 61(37):8941-8 doi:10.1021/jf403438b

Sciancalepore M, Luin E, Parato G, et al. (2012) Reactive oxygen species contribute to the promotion of the ATP-mediated proliferation of mouse skeletal myoblasts. Free radical biology & medicine 53(7):1392-8 doi:10.1016/j.freeradbiomed.2012.08.002

Siegel D, Kepa JK, Ross D (2012) NAD(P)H:quinone oxidoreductase 1 (NQO1) localizes to the mitotic spindle in human cells. PloS one 7(9):e44861 doi:10.1371/journal.pone.0044861

Solfrizzo M, Gambacorta L, Visconti A (2014) Assessment of multi-mycotoxin exposure in southern Italy by urinary multi-biomarker determination. Toxins 6(2):523-38 doi:10.3390/toxins6020523

Solhaug A, Torgersen ML, Holme JA, Lagadic-Gossmann D, Eriksen GS (2014) Autophagy and senescence, stress responses induced by the DNA-damaging mycotoxin alternariol. Toxicology 326:119-29 doi:10.1016/j.tox.2014.10.009

Soukup ST, Kohn BN, Pfeiffer E, et al. (2016) Sulfoglucosides as Novel Modified Forms of the Mycotoxins Alternariol and Alternariol Monomethyl Ether. Journal of agricultural and food chemistry 64(46):8892-8901 doi:10.1021/acs.jafc.6b03120

Stanic A, Uhlig S, Solhaug A, Rise F, Wilkins AL, Miles CO (2016) Preparation and Characterization of Cysteine Adducts of Deoxynivalenol. Journal of agricultural and food chemistry 64(23):4777-85 doi:10.1021/acs.jafc.6b01158

Tang Y, Li J, Li F, et al. (2015) Autophagy protects intestinal epithelial cells against deoxynivalenol toxicity by alleviating oxidative stress via IKK signaling pathway. Free radical biology & medicine 89:944-51 doi:10.1016/j.freeradbiomed.2015.09.012

Tima H, Bruckner A, Mohacsi-Farkas C, Kisko G (2016) Fusarium mycotoxins in cereals harvested from Hungarian fields. Food additives & contaminants Part B, Surveillance doi:10.1080/19393210.2016.1151948

Tralamazza SM, Bemvenuti RH, Zorzete P, de Souza Garcia F, Correa B (2016a) Fungal diversity and natural occurrence of deoxynivalenol and zearalenone in freshly harvested wheat grains from Brazil. Food chemistry 196:445-50 doi:10.1016/j.foodchem.2015.09.063

Tralamazza SM, Braghini R, Correa B (2016b) Trichothecene Genotypes of the Fusarium graminearum Species Complex Isolated from Brazilian Wheat Grains by Conventional and Quantitative PCR. Frontiers in microbiology 7:246 doi:10.3389/fmicb.2016.00246

Turner PC, Hopton RP, White KL, Fisher J, Cade JE, Wild CP (2011) Assessment of deoxynivalenol metabolite profiles in UK adults. Food and chemical toxicology : an international journal published for the British Industrial Biological Research Association 49(1):132-5 doi:10.1016/j.fct.2010.10.007

Turner PC, Rothwell JA, White KL, Gong Y, Cade JE, Wild CP (2008) Urinary deoxynivalenol is correlated with cereal intake in individuals from the United kingdom. Environmental health perspectives 116(1):21-5 doi:10.1289/ehp.10663

Ueno Y (1977) Mode of action of trichothecenes. Annales de la nutrition et de l'alimentation 31(4-6):885-900

Ueno Y, Matsumoto H (1975) Inactivation of Some Thiol-Enzymes by Trichothecene Mycotoxins from Fusarium Species. CHEMICAL & PHARMACEUTICAL BULLETIN 23(10):2439-2442 doi:10.1248/cpb.23.2439

van der Lee T, Zhang H, van Diepeningen A, Waalwijk C (2015) Biogeography of Fusarium graminearum species complex and chemotypes: a review. Food additives & contaminants Part A, Chemistry, analysis, control, exposure & risk assessment 32(4):453-60 doi:10.1080/19440049.2014.984244

Vlada CA, Kim J-S, Behrns KE (2015) Autophagy: Self-preservation through cannibalism of proteins and organelles. Surgery 157(1):1-5 doi: 10.1016/j.surg.2014.07.014

Walravens J, Mikula H, Rychlik M, et al. (2016) Validated UPLC-MS/MS Methods To Quantitate Free and Conjugated Alternaria Toxins in Commercially Available Tomato Products and Fruit and Vegetable Juices in Belgium. Journal of agricultural and food chemistry 64(24):5101-9 doi:10.1021/acs.jafc.6b01029

Wan D, Huang L, Pan Y, et al. (2014) Metabolism, Distribution, and Excretion of Deoxynivalenol with Combined Techniques of Radiotracing, High-Performance Liquid Chromatography Ion Trap Time-of-Flight Mass Spectrometry, and Online Radiometric Detection. Journal of agricultural and food chemistry 62(1):288-296 doi:10.1021/jf4047946

Wang XJ, Sun Z, Chen W, Eblin KE, Gandolfi JA, Zhang DD (2007) Nrf2 protects human bladder urothelial cells from arsenite and monomethylarsonous acid toxicity. Toxicology and applied pharmacology 225(2):206-13 doi:10.1016/j.taap.2007.07.016

Warth B, Del Favero G, Wiesenberger G, et al. (2016) Identification of a novel human deoxynivalenol metabolite enhancing proliferation of intestinal and urinary bladder cells. Scientific reports 6:33854 doi:10.1038/srep33854

Warth B, Fruhmann P, Wiesenberger G, et al. (2015) Deoxynivalenol-sulfates: identification and quantification of novel conjugated (masked) mycotoxins in wheat. Analytical and bioanalytical chemistry 407(4):1033-9 doi:10.1007/s00216-014-8340-4

Warth B, Petchkongkaew A, Sulyok M, Krska R (2014) Utilising an LC-MS/MS-based multi-biomarker approach to assess mycotoxin exposure in the Bangkok metropolitan area and surrounding provinces. Food additives & contaminants Part A, Chemistry, analysis, control, exposure & risk assessment 31(12):2040-6 doi:10.1080/19440049.2014.969329

Warth B, Sulyok M, Fruhmann P, et al. (2012) Assessment of human deoxynivalenol exposure using an LC-MS/MS based biomarker method. Toxicol Lett 211(1):85-90 doi:10.1016/j.toxlet.2012.02.023

Wittig A, Gehrke H, Del Favero G, et al. (2017) Amorphous Silica Particles Relevant in Food Industry Influence Cellular Growth and Associated Signaling Pathways in Human Gastric Carcinoma Cells. Nanomaterials (Basel, Switzerland) 7(1) doi:10.3390/nano7010018

Wu Q-H, Wang X, Yang W, et al. (2014) Oxidative stress-mediated cytotoxicity and metabolism of T-2 toxin and deoxynivalenol in animals and humans: an update. Archives of toxicology 88(7):1309-1326 doi:10.1007/s00204-014-1280-0

Figures and Figure captions

Figure 1

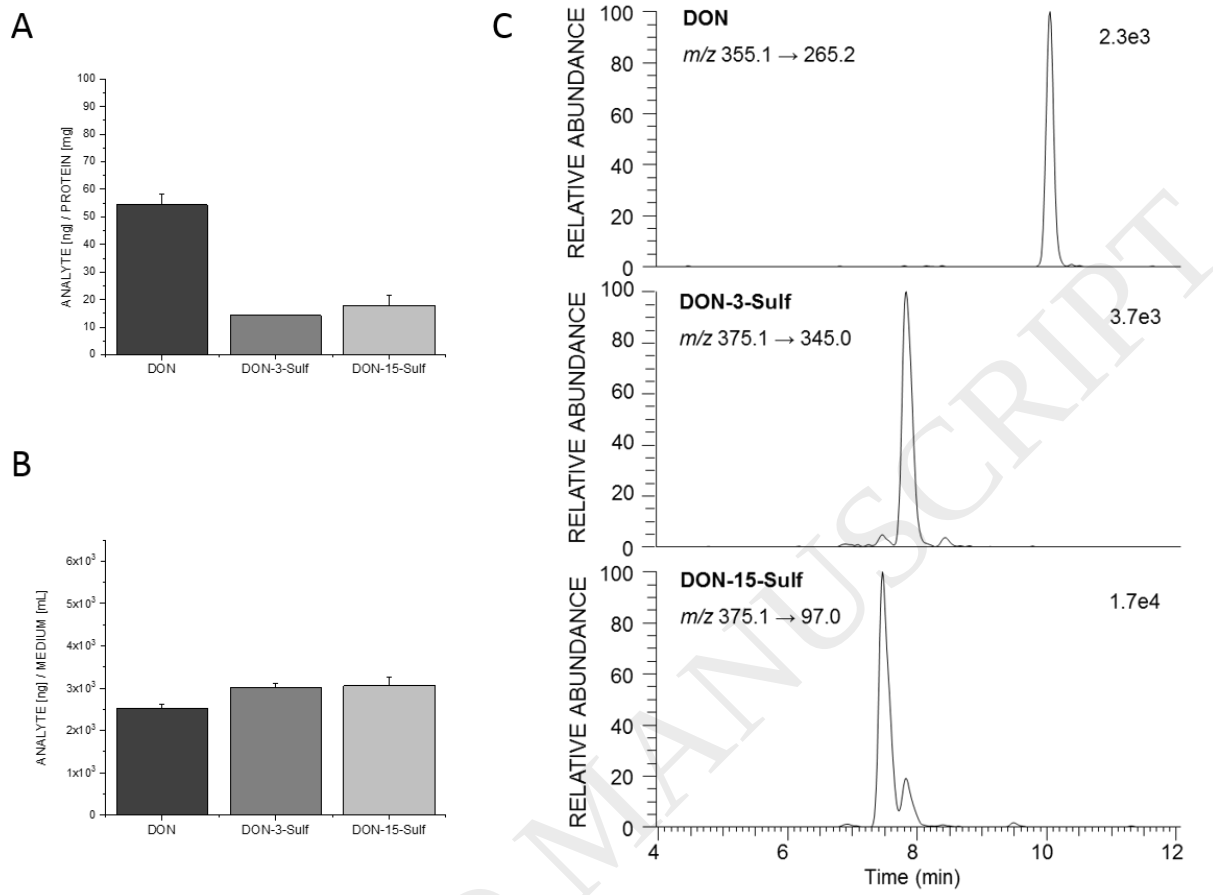

Figure 1. Intracellular and media concentrations of deoxynivalenol and its sulfates in HT-29 cultures after 24 h incubations (A) intracellular concentrations (B) concentrations in the cell culture medium, both. In (C) a MRM-chromatogram of a blank cell extract fortified with each 0.1 µM of DON, DON-3-Sulf, and DON-15-Sulf is shown to demonstrate the chromatographic separation of the compounds.

Figure 2

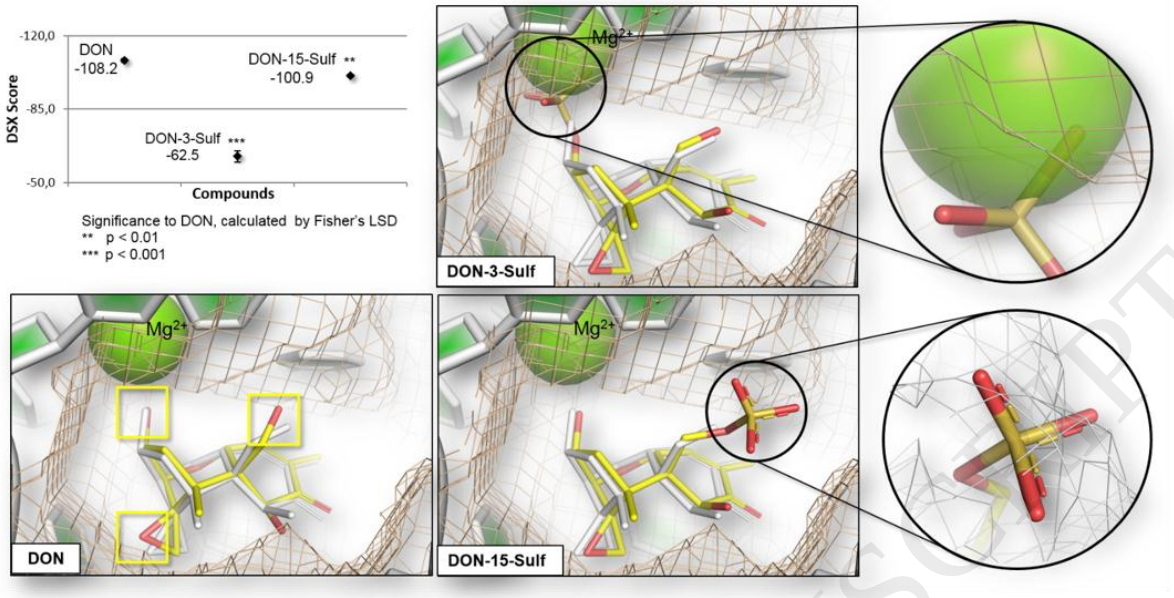

Figure 2. *In silico* results of DON and sulfate conjugates. The plot represents the computed scores of DON and sulfate conjugates. The more negative the score, the better the interaction as the DSX scoring function estimates the thermodynamic stability of intermolecular interactions (further details are reported in the Section 2.5; Material and Methods). The binding architectures represent the mode of binding of DON and sulfate conjugates in the ribosome A-site. Ligands and the rRNA forming binding site are represented in sticks, while the Mg^{2+} ion is represented in sphere. The yellow boxes indicate the DON groups involved in polar interaction with the binding site, which is outlined with the yellow mesh. All the computed poses (yellow) are superimposed to the crystallographic pose of DON (PDB structure code 4U53; Garreau de Loubresse et al. 2014). The close up of the sulfate groups of DON-3-Sulf (on the top) and DON-15-Sulf (on the bottom) is reported in the black circles. DON-3-Sulf showed a sterical clash with the Mg^{2+} ion, while DON-15-Sulf was found arranging improperly the sulfate group in a hydrophobic environment (represented by the grey mesh).

Figure 3

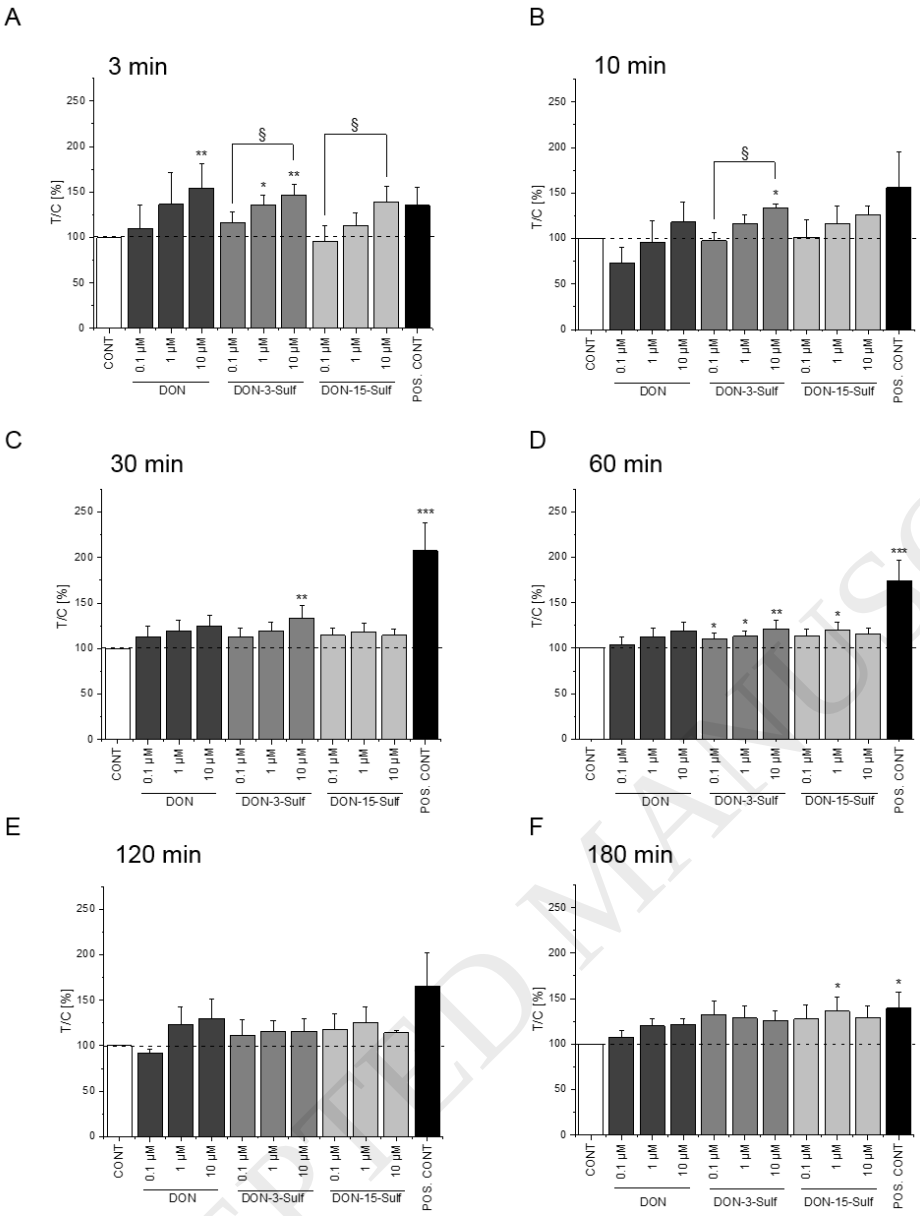

Figure 3. Potential of DON and DON-sulfates to trigger ROS levels in HT-29 cells, measured in the DCFH-DA assay. Effect of DON (dark grey), DON-3-Sulf (grey) and DON-15-Sulf (light grey) was calculated as % of controls (CONT, white bars) and compared to 500 µM H_2O_2 (POS. CONT, black bars). The incubation time in minutes was as follows: (A) 3, (B) 10, (C) 30, (D) 60, (E) 120, (F) 180. Every data point is equal to the mean ± SEM of n ≥ 5 independent biological replicates performed in hexuplicates. Data were analyzed with one-way analysis of variance (ANOVA) followed by post-hoc Fisher's LSD. Symbols indicate different distributions in comparison to controls (* 0.05 level, ** at 0.01 level, *** 0.001 level), or to the tested compounds (§ 0.05 level, §§ at 0.01 level, §§§ 0.001 level).

Figure 4

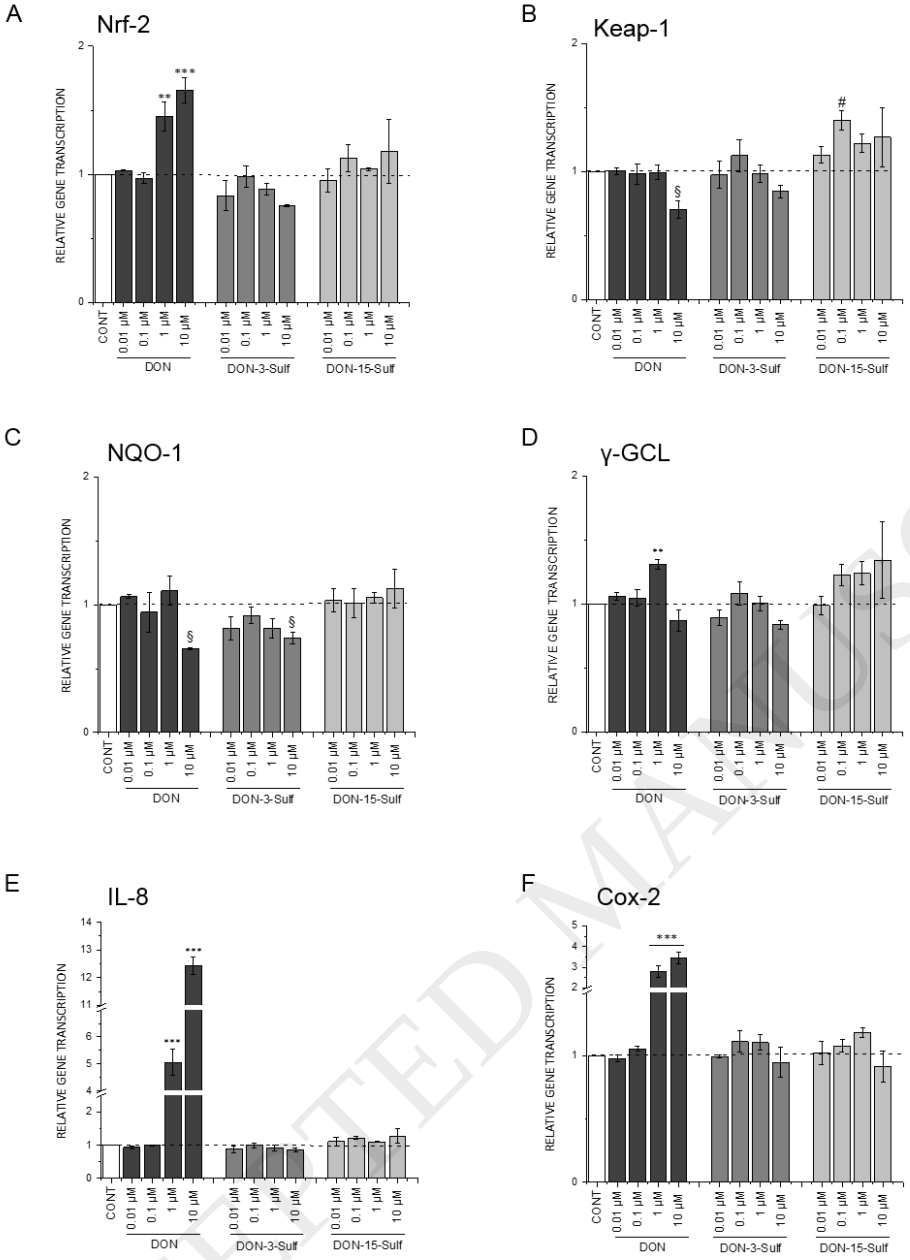

Figure 4. Impact of DON and DON-sulfates on gene transcription in HT-29 cells after 3h, measured by qPCR. Effect of DON (dark grey), DON-3-Sulf (grey) and DON-15-Sulf (light grey) was calculated as relative gene transcription in comparison to controls (white bars). (A) Nrf2; (B) Keap-1; (C) NQO-1; (D) γGCL; (E) IL-8; (F) COX-2. Data are the mean of n = 3 independent experiments ± SEM. Data were tested by independent one-way ANOVA and Fisher LSD post hoc test. Symbols indicate signal increase in comparison to controls (* 0.05 level, ** at 0.01 level, *** 0.001 level), decrease in comparison to controls (§ 0.05 level, §§ at 0.01 level, §§§ 0.001 level), or significant difference in comparison to respective concentration of DON (# 0.05 level, ## at 0.01 level, ### 0.001 level).

Figure 5

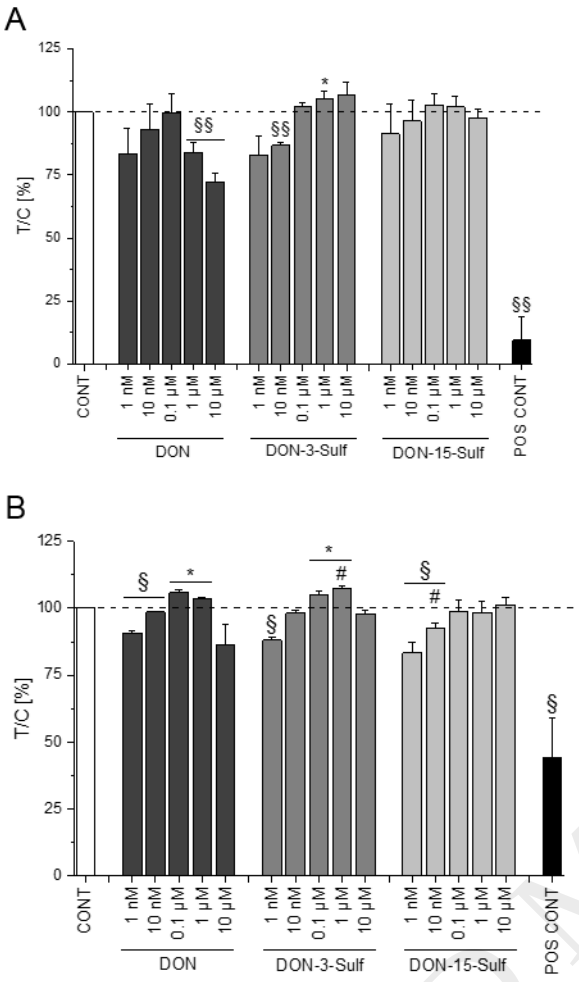

Figure 5. Cellular proliferation of DON and DON-sulfates in HT-29 cells (24 h incubation) (A) measured by WST-1 assay or (B) confluence analysis. Effects of DON (dark grey), DON-3-Sulf (grey) and DON-15-Sulf (light grey) were calculated as % of controls (CONT, white bars) and compared to the positive control (Triton X 0.1%, POS. CONT black bars). Data are the mean of n ≥ 3 independent biological replicates performed in technical quadruplicates ± SEM. Data were tested by independent one-way ANOVA and Fisher LSD post hoc test. Symbols indicate signal increase in comparison to controls (* 0.05 level, ** at 0.01 level, *** 0.001 level) or decrease in comparison to controls (§ 0.05 level, §§ at 0.01 level, §§§ 0.001 level), or difference in comparison to respective concentration of DON (# 0.05 level, ## at 0.01 level, ### 0.001 level).

Figure 6

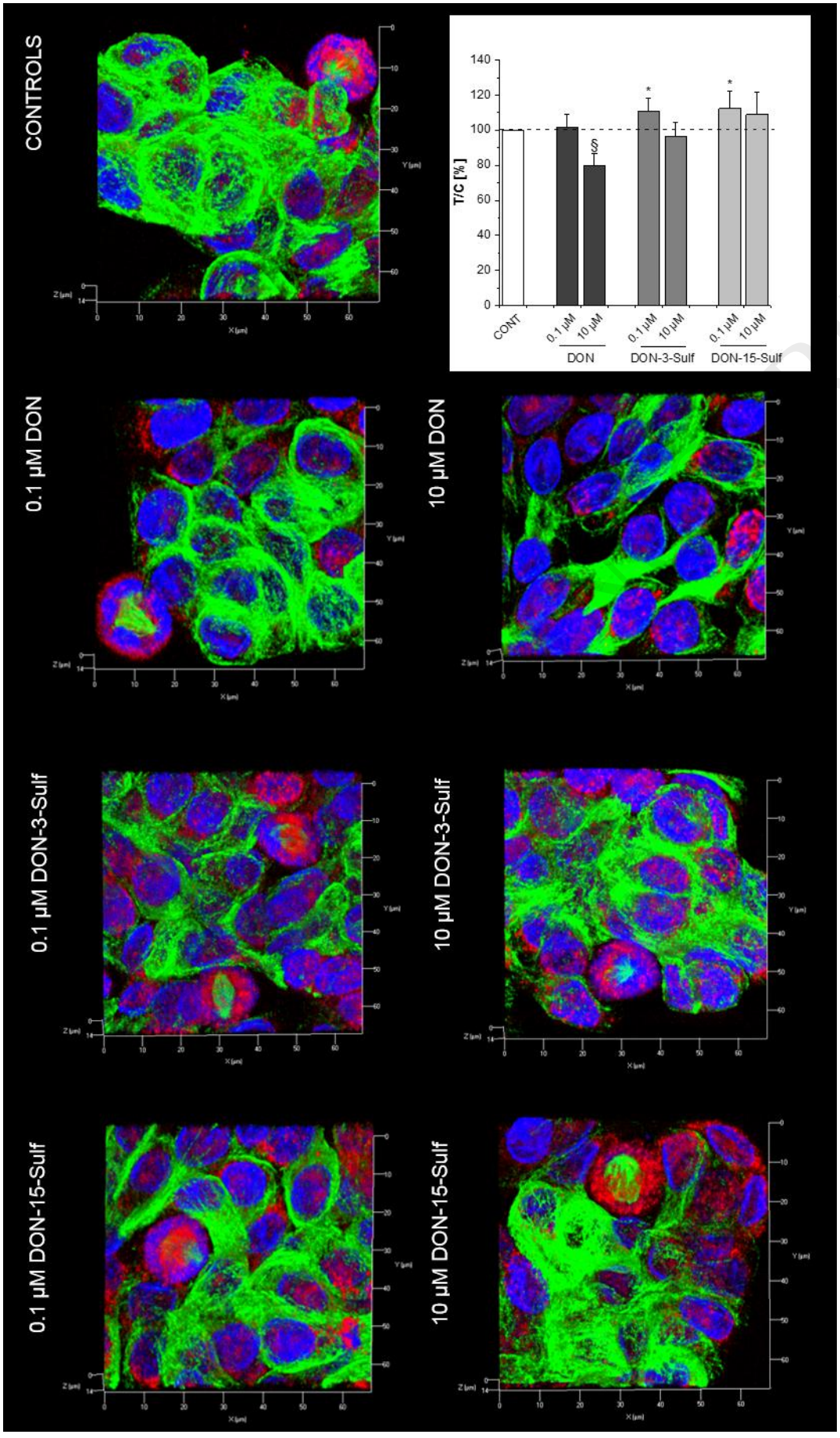

Figure 6. Immunofluorescence localization of Ki67 in HT-29 cells and evaluation of the effect of DON and DON-sulfates (0.1, 10 μM). Effect of DON (dark grey), DON-3-Sulf (grey) and DON-15-Sulf (light grey) was calculated as % of controls (CONT, white bars). Tubulin (green), Ki67 (red), cell nuclei (blue). Quantification of Ki67 signal quantified from at least 3 optical fields for every independent biological replicate (n = 4). Data were tested by Kruskal-Wallis ANOVA and Fisher LSD post hoc test. Symbols indicate signal increase in comparison to controls (* 0.05 level, ** at 0.01 level, *** 0.001 level), decrease in comparison to controls (§ 0.05 level, §§ at 0.01 level, §§§ 0.001 level), or significant difference in comparison to respective concentration of DON (# 0.05 level, ## at 0.01 level, ### 0.001 level).

Figure 7

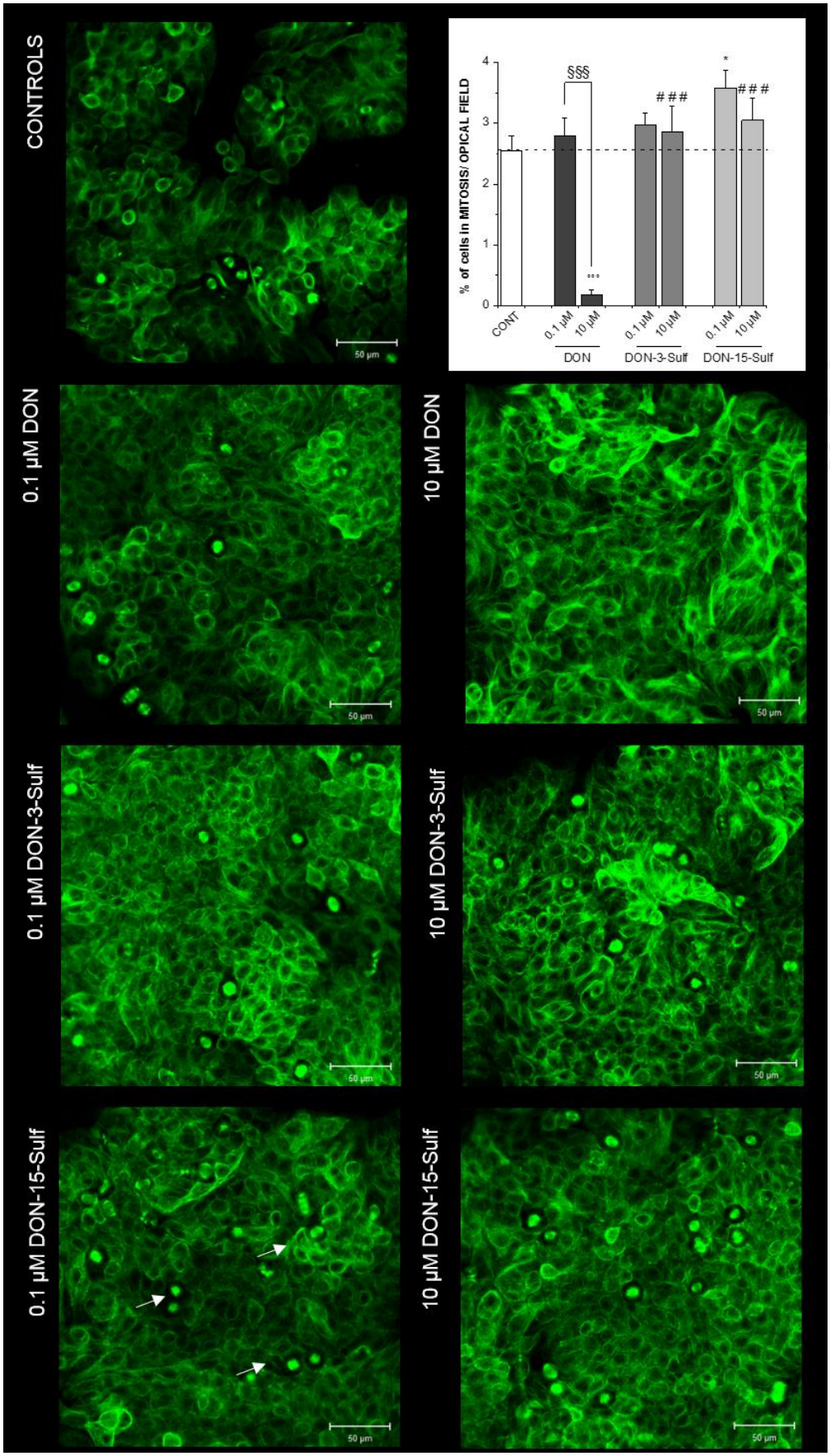

Figure 7. Microscopy image immunofluorescence localization of HT-29 cells in mitosis and evaluation of the effect of DON and DON-sulfates (0.1, 10 μM). Effects of DON (dark grey), DON-3-Sulf (grey) and DON-15-Sulf (light grey) were calculated as % cells in mitosis / optical field (controls are indicated as CONT, white bars). Tubulin (green) and mitotic spindles (white arrows). Data was obtained from at least 3 optical fields for every independent biological replicate (n = 4). Data were tested by independent one-way ANOVA and Fisher LSD post hoc test. Symbols indicate signal increase in comparison to controls (* 0.05 level, ** at 0.01 level, *** 0.001 level), decrease in comparison to controls (§ 0.05 level, §§ at 0.01 level, §§§ 0.001 level), or significant difference in comparison to respective concentration of DON (# 0.05 level, ## at 0.01 level, ### 0.001 level).

Figure 8

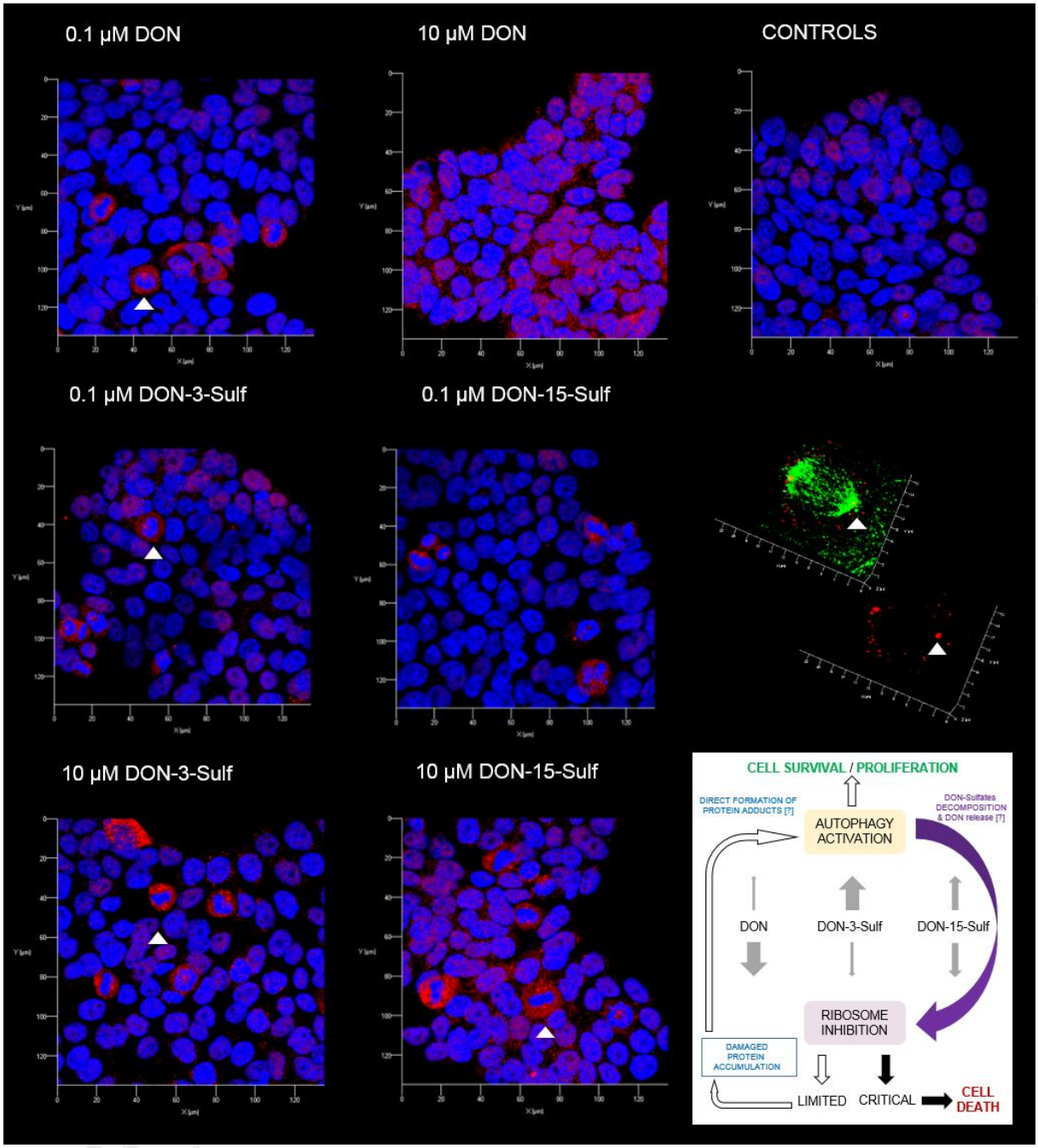

Figure 8. Confocal microscopy and SIM images of the immunofluorescence localization of LC3 in HT-29 cells and evaluation of the effect of DON and DON-sulfates (0.1, 10 µM). LC3 (red), cell nuclei (DAPI, blue) and mitotic spindle (green tubulin). Images are representative of 3 independent experiments. White arrow-heads indicate areas of accumulation of LC3 puncta. Schematic representation of the proposed interplay between ribosomal inhibition and autophagy regulation for DON and DON-3-Sulf and DON-15-Sulf.